ADVANCED MATERIALS

www.advmat.de

Anomalous Resistance Hysteresis in Oxide ReRAM: Oxygen Evolution and Reincorporation Revealed by In Situ TEM

David Cooper, Christoph Baeumer,* Nicolas Bernier, Astrid Marchewka, Camilla La Torre, Rafal E. Dunin-Borkowski, Stephan Menzel, Rainer Waser, and Regina Dittmann*

The control and rational design of redox-based memristive devices, which are highly attractive candidates for next-generation nonvolatile memory and logic applications, is complicated by competing and poorly understood switching mechanisms, which can result in two coexisting resistance hystereses that have opposite voltage polarity. These competing processes can be defined as regular and anomalous resistive switching. Despite significant characterization efforts, the complex nanoscale redox processes that drive anomalous resistive switching and their implications for current transport remain poorly understood. Here, lateral and vertical mapping of O vacancy concentrations is used during the operation of such devices in situ in an aberration corrected transmission electron microscope to explain the anomalous switching mechanism. It is found that an increase (decrease) in the overall O vacancy concentration within the device after positive (negative) biasing of the Schottky-type electrode is associated with the electrocatalytic release and reincorporation of oxygen at the electrode/oxide interface and is responsible for the resistance change. This fundamental insight presents a novel perspective on resistive switching processes and opens up new technological opportunities for the implementation of memristive devices, as anomalous switching can now be suppressed selectively or used deliberately to achieve the desirable so-called deep Reset.

Dr. D. Cooper, Dr. N. Bernier
Université Grenoble Alpes
F-38000 Grenoble, France
E-mail: david.cooper@cea.fr
Dr. D. Cooper, Dr. N. Bernier
CEA, LETI, Minatec Campus
F-38054 Grenoble, France
Dr. C. Baeumer, Prof. R. E. Dunin-Borkowski, Dr. S. Menzel, Prof. R. Waser, Prof. R. Dittmann
Peter Gruenberg Institute
Forschungszentrum Juelich GmbH and JARA-FIT
52425 Juelich, Germany
E-mail: c.baeumer@fz-juelich.de
A. Marchewka, C. La Torre, Prof. R. Waser
Institute of Electronic Materials
IWE2
RWTH Aachen University
52056 Aachen, Germany
Prof. R. E. Dunin-Borkowski
Ernst Ruska-Centre for Microscopy and Spectroscopy with Electrons
Forschungszentrum Juelich GmbH and RWTH Aachen University
52425 Juelich, Germany

DOI: 10.1002/adma.201700212

In order to meet the high demand for the high-density and low-cost future data storage and logic circuits that are required for an ever increasingly interconnected world, novel devices and new modalities of operation are required.[1] Memristive devices for redox-based resistive switching random access memory (ReRAM) are therefore intensively investigated as they present one of the most attractive emerging memory technologies.[2–5] Excellent device performance that combines fast switching, long retention and high-density stacking has already been demonstrated. But although significant progress in the understanding of resistive switching phenomena was achieved in recent years,[2] research and development is still mainly based on purely empirical strategies, rather than on predictive concepts.[6] At the heart of this roadblock lies an inadequate understanding of the nanoscale redox phenomena that are believed to be the underlying mechanism that allows switching between a high resistance state (HRS) and a low resistance state (LRS).

A prominent example of a lack of knowledge about resistive switching processes is the occurrence of competing switching mechanisms in one and the same device, which can lead to two coexisting resistance hystereses of opposite voltage polarity, i.e., the device can be set to the LRS using both positive and negative voltages, depending on the magnitude of the applied voltage. These opposing switching mechanisms have been observed, for example, in memristive devices based on TiO_x,[7,8] HfO_x,[9,10] TaO_x,[11] and $SrTiO_3$[12–16] thin films. Typically, resistive switching in such so-called valence change memories is caused by an internal redistribution of oxygen vacancies within a switching filament at the Schottky-type electrode/oxide interface.[2] This redistribution gives rise to a resistance hysteresis of normal (counter-eightwise) polarity, whereby a device can be set to the LRS by applying a negative voltage, while a positive voltage resets the device to the HRS. (Here, all voltages are given with respect to the Schottky-type (e.g., Pt) electrode.) However, resistance changes can also be driven by a second mechanism in the same device, giving rise to a resistance hysteresis of opposite

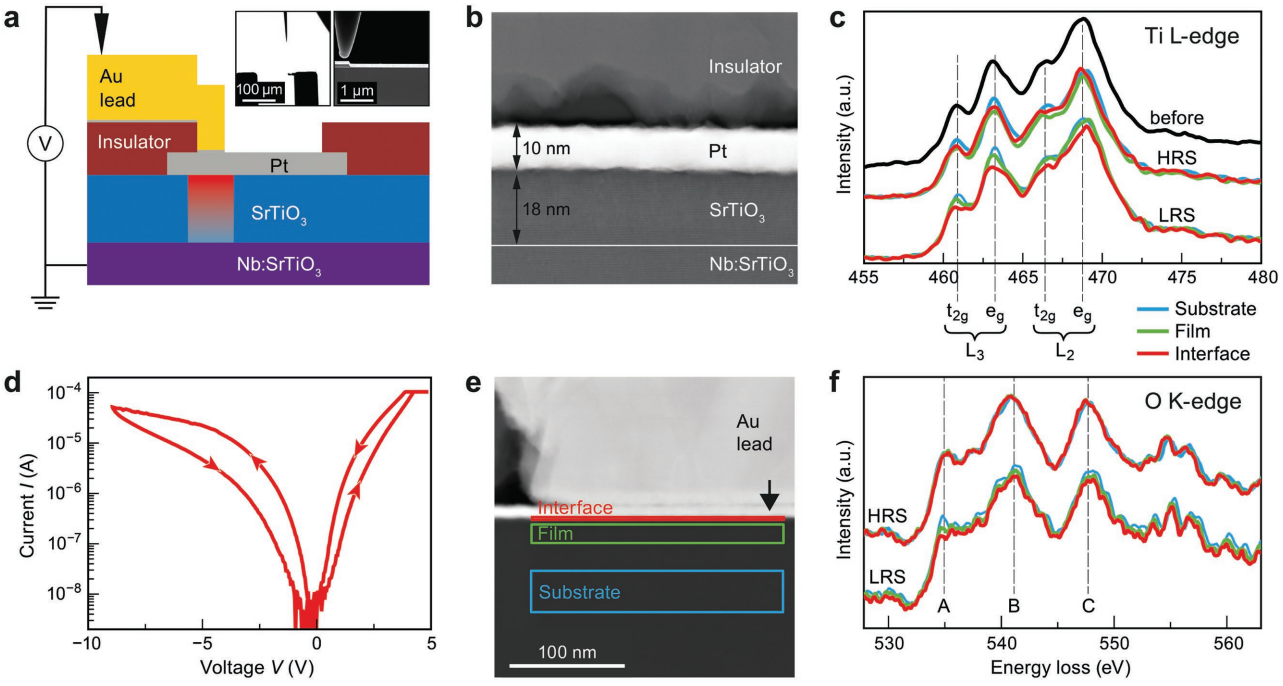

Figure 1. In situ memristive operation of an $SrTiO_3$ device in a TEM. a) Schematic of the specimen examined. The switching filament where we found switching-induced changes is shown in red. Insets: very low magnification STEM image of the specimen and electrical contact (left) and slightly larger magnification of the specimen and electrical contact (right). The insets are also shown in Figure S1 (Supporting Information). b) Higher magnification HAADF STEM image showing the geometry of the device. c) Ti L-edge EEL spectra for the regions indicated in (e), acquired before and during switching with the device in the LRS and HRS. d) *I–V* characteristics of the device, as examined in the TEM. Positive and negative voltages applied to the Pt electrode lead to a smooth Set and Reset operation, respectively. For the Set operation, a current compliance of 100 µA was used. e) STEM image showing the region examined during the switching experiment. The different zones that were examined are labeled. f) O K-edge EEL spectra for the same regions as in (c). Although the oxygen spectra are noisy relative to the Ti spectra, a reduction in the peak "A" intensity can be observed in the LRS, indicating an increased number of electrons in the conduction band, i.e., an increased amount of Ti^{3+}(ref. [29]).

(eightwise) polarity. The origin of this anomalous switching polarity and its implications for device operation are still not understood.

This lack of understanding has been related primarily to the absence of an analysis method that can be used to provide information about electronic and chemical structure with sufficient spatial resolution and sensitivity to detect small variations at the nanometer scale. This roadblock can now be overcome using new transmission electron microscopy (TEM) techniques and instrumentation. Unfortunately, for TEM specimens that have been switched ex situ, it is very challenging to place the active region of a device within the thickness of a TEM specimen (typically 100 nm or less), while problems with volatility over time[17] or during specimen preparation[18] can result in information loss. Most importantly, small changes in specimen preparation and experimental procedure can lead to difficulties in accurately interpreting analytical data. In order to overcome these problems, we used in situ scanning TEM (STEM) and electron energy-loss spectroscopy (EELS) to image and characterize the active region in the same device in both resistance states, in order to unveil the fundamental redox processes that underlie eightwise resistive switching. We examine $SrTiO_3$, which can be considered a model material because of its well understood defect chemistry and feasible fabrication as an epitaxial thin film, i.e., a grain-boundary-free platform with a low defect density. The $SrTiO_3$ layer is sandwiched between a degenerately Nb-doped $SrTiO_3$ ($Nb:SrTiO_3$) bottom electrode with metallic conductivity, yielding an almost ohmic contact, and a Pt top electrode, which presents a Schottky barrier to $SrTiO_3$.

As a result of its potential for atomic-scale imaging of physical and chemical processes, there has recently been considerable progress in the development of in situ TEM using piezo-controlled electrical probes and great interest in its application to memristive devices.[19–26] Most previous reports on valence change memories have been based on the use of TEM or STEM imaging and diffraction. Although they revealed changes during switching, they did not provide quantitative physicochemical information about the switching mechanisms, as they did not make use of analytical TEM techniques such as EELS to measure changes in atomic concentration or electronic states during switching. In addition, the electrical contact point is frequently applied directly to the region of interest, which can cause destructive local heating effects and mechanical stress.[20] As such extrinsic effects need to be prevented to study fundamental resistive switching processes,[23] the key to successful in situ memristive operation in a TEM is careful positioning of the electrical contact. Therefore, in the present study we chose to operate a $Pt/SrTiO_3/Nb:SrTiO_3$ device in a specimen of thickness ≈100 nm in situ in the TEM by contacting it electrically far from the actual device area, using a contact pad that was located on a thicker part of the specimen and connected to the active device through a lithographically defined metal lead (**Figure 1**a,b and Supporting Information).

High-angle annular dark-field (HAADF) STEM images (Figure 1b) and EEL spectra were acquired before the switching experiment to measure the device in the unformed state. A representative Ti L-edge EEL spectrum acquired in the pristine state confirms the presence of homogeneous, fully oxidized $SrTiO_3$ (mainly Ti^{4+} states, Figure 1c). The device was then switched between the LRS and HRS in an eightwise hysteresis direction by sweeping to positive and negative voltages, respectively (Figure 1d). In order to protect the lamella from excessive Joule heating, a comparably low current compliance of 100 µA was used. Before and after each switching event, the entire active device area was mapped using EELS. The oxidation state in each region of the device could then be obtained from the intensities and positions of the different characteristic peaks in the EEL spectra.[27–29] Figure 1e shows an HAADF STEM image of the region of interest with the substrate, film and $Pt/SrTiO_3$ interface regions indicated. The Ti L-edge after switching to the LRS and the HRS is shown in Figure 1c. For the device in the HRS, it is clear that there are only small changes in the Ti spectra when compared with the pristine state for the entire device. However, for the LRS there are reductions in intensity and shifts of the characteristic peaks, corresponding to a reduction in Ti^{4+} states and an increase in Ti^{3+} states, as is apparent from a decrease of the L_3 t_{2g} peak and a slight shift and broadening of the other peaks.[30] This trend is confirmed by changes in the O K-edge spectra in the same regions (Figure 1f). In order to verify the reproducibility of these results and that they did not result from irreversible heating effects, the device was switched between the LRS and HRS several times and further spectra were acquired, resulting in the same observations (Figure S2, Supporting Information). We also verified that the LRS retention inside the microscope was sufficiently stable for our measurements by reading out the resistance after several days. This demonstrates that the observed changes are due to nonvolatile switching effects.

The oxidation states in the device were then mapped with high spatial resolution. **Figure 2**a shows an annular dark-field (ADF) STEM image of the region of interest in the LRS, while Figure 2b,c shows EEL spectra collected from the ≈20 nm $SrTiO_3$ thin film from the substrate toward the Pt interface in steps of 1.2 nm for both the LRS and the HRS. A gradual shift and broadening of the L_3 e_g peak is visible in Figure 2b, indicating a gradual change in the Ti^{3+}/Ti^{4+} ratio in the LRS. This trend becomes more obvious when the normalized intensity of the L_3 t_{2g} edge is plotted (Figure 2d), providing a direct measure of the oxidation state of the device.[30,31] The fact that this valence change is caused by oxygen vacancies is evident from the oxygen concentration profile obtained by integrating the oxygen EELS edge (Figure 2d). The oxidation state is modified most strongly near the Pt electrode, where the L_3 e_g edge is shifted by –0.3 eV. This shift is indicative of a decrease in oxygen-vacancy concentration of up to 4 at%.[30] A map of the L_3 e_g peak width indicates changes in Ti^{3+} concentration in a two-dimensional manner (Figure 2e). For the LRS, the Ti^{3+} concentration appears only in the $SrTiO_3$ film, increasing linearly from the bottom to the

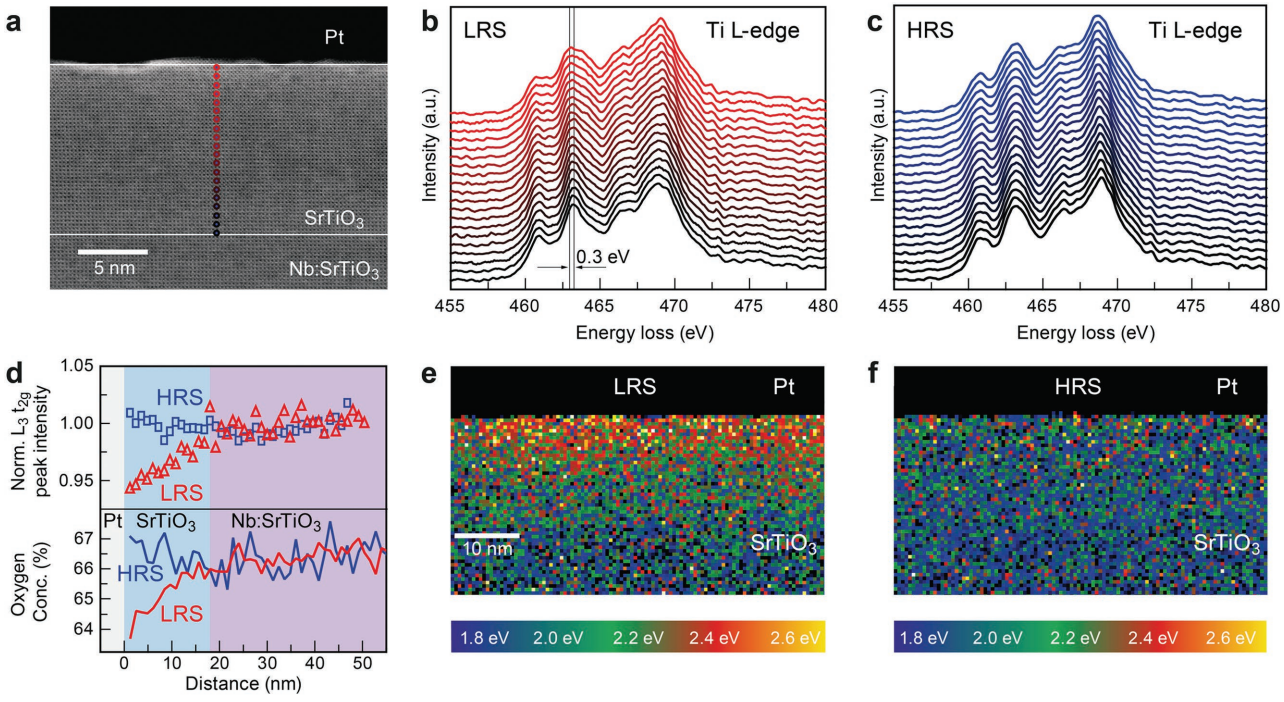

Figure 2. Vertical mapping of the redox reaction. a) High-resolution ADF STEM image of the region of interest in the LRS. b) Ti L-edge EEL spectra for the device in the LRS. The spectra were acquired across the $SrTiO_3$ film in 1.2 nm steps from the bottom to the top, as indicated in (a). They show the evolution of the edges as a function of position up to a depth of 20 nm into the device. c) Ti L-edge EEL spectra for the device in the HRS. Again, the spectra were acquired across the $SrTiO_3$ film in 1.2 nm steps from the bottom to the top, as indicated in (a). d) Upper panel: intensity of the L_3 e_g edge as a function of depth into the specimen for the LRS and HRS to a depth of 55 nm into the device. Lower panel: oxygen concentration profiles acquired by integrating the oxygen EELS edge for the same region in the HRS and LRS. e) Map of the fitted Ti L_3 e_g peak width in the LRS. f) Map of the fitted Ti L_3 e_g peak width in the HRS.

top, while it is rather homogeneous laterally. A comparison of this trend in Ti^{3+}/Ti^{4+} ratio for the LRS with the same measurement for the HRS reveals that in the HRS the entire film shows only Ti^{4+} states and no oxygen deficiency (Figure 2c,d,f), confirming that a valence change at the $Pt/SrTiO_3$ interface is the origin of the eightwise memristive operation. Since operation at high current densities may lead to the formation of Sr-rich secondary phases in $SrTiO_3$ devices,[17,32] we would like to note that, to within experimental resolution, we did not find evidence for Sr or Ti movement during the switching between a LRS and a HRS. Regarding the location and the horizontal extent of the switching filament, a detailed investigation is provided in the Supporting Information (Figures S3–S5). In accordance with our previous reports on eightwise switching in $SrTiO_3$, we found filamentary switching (compare Figure 1a) with a rather large (μm-sized) filament.[12,17,29]

As direct experimental observation of the redox states in the LRS and HRS has been inaccessible, several models have been suggested to explain the anomalous switching phenomenon, as described below. Our nanoscale insight about the redox reaction during eightwise resistive switching obtained using in situ TEM characterization now allows us to evaluate each of the proposed mechanisms.

Mechanism 1: Since the regular switching can be explained well through the motion of oxygen vacancies, it was suggested that anomalous switching is related to purely electronic effects instead, such as charge trapping mechanisms which may alter the effective Schottky barrier.[16,33,34] But as our results clearly demonstrate a change in oxygen-vacancy concentration during switching, purely electronic effects are not responsible for the resistance change observed here. Instead, the frequently observed change of the Schottky barrier[16] is a result of the change in oxygen-vacancy concentration.[29,35,36] As shown in our previous work, the change in oxygen-vacancy concentration observed here can fully account for orders of magnitude in device resistance.[29]

Mechanism 2: Since we showed in our earlier work that the $Nb:SrTiO_3/SrTiO_3$ interface is not free from space charge,[37] a possible explanation for anomalous switching could involve resistive switching taking place at the bottom electrode interface instead of at the top Pt interface because of an increased potential barrier modulated by the near-interface oxygen-vacancy concentration ($[V_{\ddot{O}}]$, using the Kröger-Vink notation[38]) (**Figure 3**a,b) as was suggested for many other systems as well.[7,39] Here, the potential barrier at the bottom electrode interface would have to be larger than that at the top electrode interface in order to dominate the *I–V* characteristics of the device. However, for this scenario to be true, we would expect high $[V_{\ddot{O}}]$ near the $Nb:SrTiO_3/SrTiO_3$ interface in the LRS, whereas our experimental results indicate exactly the opposite, i.e., oxygen-vacancy accumulation at the Pt interface.

Mechanism 3: When oxygen vacancies are attracted to the top electrode and are highly concentrated near the interface, then the region below may become oxygen-vacancy-deficient (Figure 3c). The increased resistance of this region then causes the HRS.[12,40,41] However, $[V_{\ddot{O}}]$ would need to be highest near the interface for the HRS, which is opposite to the flat $[V_{\ddot{O}}]$ distribution in the HRS and the $[V_{\ddot{O}}]$ increase in the vicinity of the Pt electrode in the LRS observed in our results. Therefore, Mechanism 3 cannot account for anomalous resistive switching in these samples.

As these suggested mechanisms do not agree with our experimental Ti^{3+} profiles for the LRS and HRS, we investigated the evolution of the corresponding oxygen-vacancy distributions upon electrical bias using a numerical drift-diffusion model of coupled electronic-ionic transport inside the oxide layer (see Supporting Information for details).[42] In the simulations, both electrodes are considered to be oxygen blocking, enabling a mere redistribution of the donor-type oxygen-vacancies inside the oxide layer. Starting with the homogeneous oxygen-vacancy distribution of the HRS (Figure 3d), a positive triangular voltage signal is applied, resulting in the (intuitively expected) retraction of oxygen vacancies from the Pt interface. Such a distribution is associated with an increased Schottky barrier and therefore an increased device resistance (Figure 3e,f). This behavior, which in fact corresponds to the regular counter-eightwise switching mechanism, is in stark contrast to our experiments, in which the $SrTiO_3$ device is switched to the LRS in the presence of a positive bias, with an increased concentration of Ti^{3+} at the Pt electrode interface, corresponding to an increased $[V_{\ddot{O}}]$.

The evolution of the oxygen-vacancy profile of the LRS upon application of a negative triangular voltage signal was also simulated (Figure 3g,i). A further increase in $[V_{\ddot{O}}]$ was observed near the Pt electrode interface, while the concentration at the $Nb:SrTiO_3$ electrode decreased. The resulting distribution does not resemble the flat distribution of the HRS in our experimental data. In conclusion, pure redistribution of oxygen vacancies inside the oxide—one of the basic assumptions of many resistive switching models—leads solely to counter-eight wise resistive switching and completely fails to explain eightwise resistive switching, as the observed donor profiles for the LRS and HRS cannot be transformed into each other.

Based on the shortcomings of these existing models, we propose the following model for eightwise switching, which is in excellent agreement with our experimental results.

Mechanism 4: As the total oxygen-vacancy concentration in the entire $SrTiO_3$ film (and not just at one interface) varies reversibly between a high concentration after applying a positive voltage (Set to LRS) and a low concentration after applying a negative voltage (Reset to HRS), oxygen must inevitably be removed from the $SrTiO_3$ lattice at the Pt electrode interface during the Set process and reincorporated during the Reset, as shown schematically in **Figure 4**. This behavior is verified experimentally by the total oxygen concentration difference of the device in the LRS and HRS (Figure 2d). In other words, a positive bias on the Pt electrode results in anodic oxidation of lattice oxygen and in the formation of oxygen vacancies in the vicinity of the $Pt/SrTiO_3$ interface and the evolution of oxygen gas. This reaction leaves behind two electrons, as observed experimentally in the form of a valence change between Ti^{4+} and Ti^{3+}

$$O_O^x \rightarrow V_{\ddot{O}} + 2e' + \frac{1}{2}O_2 \quad (1)$$

$$2\,Ti^{4+} + 2e^- \rightarrow 2\,Ti^{3+} \quad (2)$$

In the same sense, a negative bias results in a reduction reaction at the $Pt/SrTiO_3$ interface

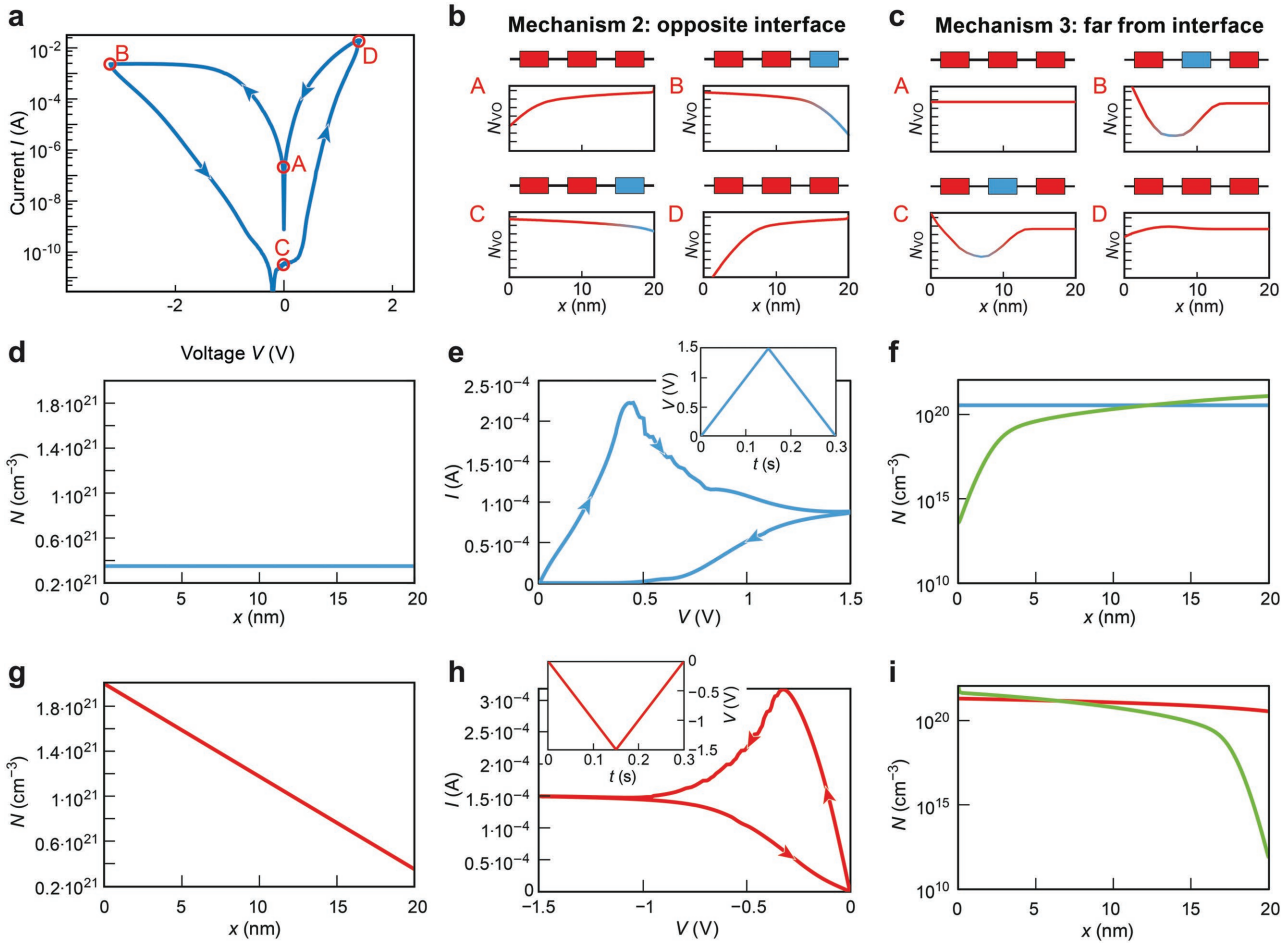

Figure 3. Limitations of previous attempts to explain eightwise switching in $SrTiO_3$. a) Exemplary *I–V* curve of a typical µm-sized device exhibiting eightwise switching. b) Proposed mechanism for switching at the bottom electrode interface located at $x = 20$ nm. Schematic oxygen-vacancy concentration N_{VO} A) in the LRS, B) during Reset, C) in the HRS, and D) during Set based on ref. [42]. c) Proposed mechanism for switching far from the top electrode interface located at $x = 0$ nm. Schematic oxygen-vacancy concentration N_{VO} A) in the LRS, B) during reset, C) in the HRS, and D) during Set based on the mechanism proposed in ref. [12]. The resistance of the top interface, the $SrTiO_3$ layer itself, and the bottom interface are represented by electronic symbols for simple resistors connected in series. Low resistance is indicated in red and high resistance is indicated in blue. d) Oxygen-vacancy profile of the HRS derived from the experiments. e) Simulated *I–V* curves for a triangular signal of positive voltages, using the vacancy profiles from (d) as initial donor concentration profiles. f) Simulated vacancy profiles before and after the application of the positive voltage signal (blue line and green line, respectively). g) Oxygen-vacancy profile of the LRS derived from the experiments. h) Simulated *I–V* curves for a triangular signal of negative voltages using the vacancy profiles from (g) as initial donor concentration profiles. i) Simulated vacancy profiles before and after the application of the negative voltage signal (red line and green line, respectively).

$$V_{\ddot{O}} + 2e' + \frac{1}{2}O_2 \rightarrow O_O^x. \quad (3)$$

From an electrochemical perspective, these processes can be regarded as oxygen evolution and oxygen reduction reactions.[43]

To verify that such electrochemical processes are not an artifact from device operation in a TEM, similar devices were also operated in dry gas atmospheres of varying oxygen partial pressure (Figure S6, Supporting Information). The R_{off}/R_{on} ratio is largest in oxidizing atmospheres, indicating exchange with the surroundings and verifying the mechanism that was derived from our TEM results. While the triple phase boundary ($SrTiO_3$/Pt/vacuum) at the lamella edge may play a role for the oxygen evolution inside the TEM, these devices do not exhibit a triple phase boundary with the surrounding atmosphere. Therefore, the oxygen is evidently (partially) stored within the Pt electrode and not completely removed from the devices, as they are operational in reducing atmospheres and in a vacuum inside the TEM (with a less efficient Reset for both cases). Migration and storage of oxygen species within Pt electrodes has already been shown many years ago,[44–46] most probably as an effect of physisorption or chemisorption within grain boundaries. Nevertheless, the exact details of the oxygen evolution and reduction reactions at the interface under applied bias as well as the influence of the electrode's microstructure and the influence extrinsic species such as water or adsorbed carbon species have to remain a subject of future research.

There have already been indications and considerations that oxygen evolution and reincorporation can also drive resistance change in other valence change memristive systems, such as

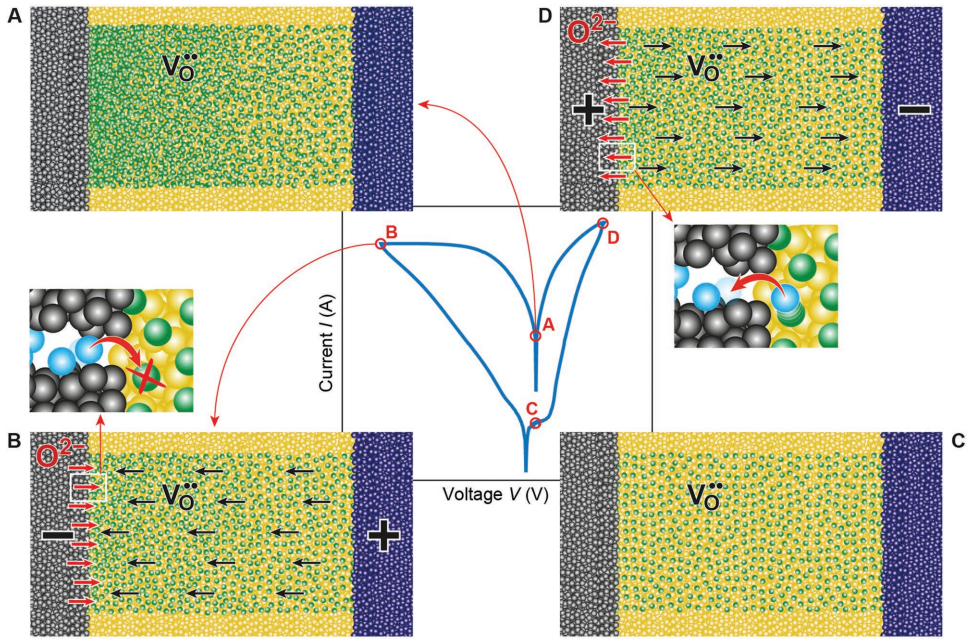

Figure 4. Proposed mechanism for anomalous switching through oxygen evolution and reincorporation of oxygen. An exemplary *I–V* curve of a similar device exhibiting anomalous switching is depicted together with schematics of the proposed mechanism. A) LRS. Oxygen-vacancy filament (green circles) in a matrix of stoichiometric $SrTiO_3$ (yellow circles) sandwiched between a Pt top electrode (gray circles) and a Nb:$SrTiO_3$ bottom electrode (blue circles). B) Reset operation. Oxygen ions are reincorporated into the $SrTiO_3$ lattice at the Pt electrode and recombine with the oxygen vacancies, reducing the total number of vacancies in the filament. C) HRS. The filament is nearly completely re-oxidized. D) Set. Oxygen ions are removed from the $SrTiO_3$ lattice at the Pt electrode, leaving behind oxygen vacancies.

WO_{3-x},[47] TiO_2,[8] Si-rich SiO_x,[48,49] Nb:$SrTiO_3$,[50] CeO_2,[21] $SrRuO_3$,[11] $La_{0.8}Sr_{0.2}MnO_3$,[51] $Pr_{0.67}Ca_{0.33}MnO_3$,[52] and the technologically relevant HfO_x[9,10] and TaO_x.[11] However, most of these reports were based on the interpretation of *I–V* curves (except for the detailed investigation in ref. [21]), while we now provide direct spectroscopic verification of the redox states in the LRS and HRS. Oxygen evolution and reincorporation remained largely ignored for the understanding and modeling of memristive devices and, accordingly, for their development toward applications. Hence, our direct observation of the valence change induced by the oxygen evolution and oxygen reduction reaction demonstrates a fundamentally important insight into redox-based memristive devices in general. In fact, we believe this is a similar situation as the recently proposed resistive switching with oxidizable electrodes based on electrochemical electrode reactions.[53]

At first sight, a switching mechanism that is based on oxygen evolution and reincorporation is technologically challenging due to exchange with the environment, as purely internal redistribution (i.e., counter-eightwise switching) might be favorable to improve device stability. Accordingly, the development of an understanding of the origin of eightwise resistive switching can help to design memristive devices by educated means through the suppression of eightwise switching. This suppression could be achieved, for example, through engineering of defect density, film thickness and operating conditions, in order to develop intentional architectures that enhance internal redistribution and suppress oxygen exchange. For example, eightwise switching typically requires higher operating voltages than counter-eightwise switching (Figure S7, Supporting Information). Operation at low voltages—which can be understood based on our results as operation below the critical voltage for oxygen evolution and reincorporation—can therefore suppress eightwise switching.

On the other hand, the HRS obtained with oxygen-exchange driven switching is higher than the HRS for counter-eightwise switching in the same cells, frequently leading to higher R_{off}/R_{on} ratios for eightwise switching (see Figure S7 in the Supporting Information as an example). In other words, reoxidation of the entire switching filament yields a more complete, deeper Reset compared to the pure redistribution of vacancies. Such a deep reset is desirable for fast and easy access in an integrated circuit.[54] We would like to note that a similarly deep Reset can be obtained when electrochemical reactions with oxidizable electrodes occur.[55] The use of such electrochemical mechanisms therefore provides opportunities as well as challenges for technological implementation.

In conclusion, our insights derived from in situ TEM analysis provide an explanation for the long-debated anomalous eightwise switching and coexistence of two switching polarities in oxide memristive devices. In our model material $SrTiO_3$, electrochemical oxygen evolution and oxygen reduction reactions, rather than the typically invoked internal redistribution of oxygen-vacancies, give rise to eightwise switching. While oxygen evolution has already been accepted as a mechanism for electroforming, the reincorporation of oxygen (i.e., the oxygen reduction reaction) has long been neglected in this material system and in resistive switching oxides in general. However, the observed difference in total oxygen-vacancy concentration between the LRS and HRS provides indisputable

evidence for this mechanism and demonstrates a route toward a deep Reset, which is desirable for technological implementation. At the same time, an understanding of the origin of eight-wise switching will enable the educated design of memristive devices.

Experimental Section

Experiments were performed using a double-aberration-corrected FEI Titan Ultimate TEM equipped with a high brightness electron source and a Gatan Tridiem energy filter equipped with Dual EELS. The probe corrector was used to obtain a beam current of 200 pA while maintaining nanometer resolution. Specimens were characterized using HAADF and ADF STEM and EELS before the switching experiments. The device was cycled between the HRS and LRS several times and then left in an HRS, before immediately acquiring HAADF/ADF STEM images and EEL spectra. The EEL spectra were acquired using dual EELS, where the low loss region was recorded over the range −20 to 200 eV and the core loss region was recorded over the range 400–600 eV at a dispersion of 0.1 eV pixel^{-1}. The specimen was then switched to an LRS and EEL spectra were acquired. The EEL spectra were examined using only standard tools included in Gatan Digital Micrograph software. The only processing steps that were used involved aligning the spectra using the zero loss peak and removing plural scattering.

Oxygen maps were obtained using standard EELS signal integration techniques. However, it was found that removal of the background could lead to large errors in quantitative measurements of concentrations and that these measurements could be unreliable (Figure 2d). This is especially true for $SrTiO_3$, where the Ti and oxygen edges are close to one another. Therefore, we focused on the observation of the fine structure in the Ti spectra, which allows quantitative analysis of small changes. In order to provide maps of changes in Ti—O bonds in the region of interest, we fitted the Ti spectra to Lorentzian functions using custom software written in Matlab. Noise in the experimental data and the complex form of the Ti spectra meant that the best-fitting data were provided by the width of the L_3 e_g edge, which was used to provide maps of changes in Ti^{4+}/Ti^{3+} distribution in the active regions (Figure 2e,f).

It was found that the electron beam did not affect the $I(V)$ characteristics of the device. In addition, no current was generated by the electron beam when it was incident on the specimen. The specimen was switched ten times and then returned to a HRS and a LRS, so that additional EEL spectra could be acquired to assess the reproducibility of the results (Figure S2, Supporting Information). The experiments were repeated on a second device to ensure that the method is reproducible. These types of devices were examined extensively using in situ TEM with a range of different techniques, including off-axis electron holography for electrostatic potential mapping and energy dispersive X-ray spectroscopy for elemental analysis. It was found that STEM EELS was the most appropriate tool for assessing redox changes during the switching process.

Supporting Information

Supporting Information is available from the Wiley Online Library or from the author.

Acknowledgements

D.C. and C.B. contributed equally to this work. Funding from the DFG (German Science Foundation) within the collaborative research centerSFB 917 “Nanoswitches” is gratefully acknowledged. D.C. thanks the European Research Council for funding through Stg306535 “Holoview”. C.B. and R.D. gratefully acknowledge funding from the W2/W3 program of the Helmholtz association. The authors thank Dr. Christian Rodenbücher and Prof. Kristof Szot for help with thermal imaging, Dr. Annemarie Köhl for the *I–V* curves in Figure S7 (Supporting Information) and Philipp Michael Müller for the *I–V* curves in Figure S6 (Supporting Information). D.C., C.B., and R.D. conceived and designed the experiments. D.C. and C.B. fabricated the samples. D.C. performed the TEM experiments. D.C. and N.B. analyzed the TEM data. A.M. performed the drift-diffusion simulations. C.L.T. performed the electrothermal simulations. D.C., C.B., S.M., R.W., and R.D. interpreted the results. C.B. wrote the manuscript. R.D.B., S.M., R.W., and R.D. supervised the research. All the authors discussed the results and contributed to the manuscript.

Conflict of Interest

The authors declare no conflict of interest.

Keywords

anomalous switching, in situ TEM, memristive devices, oxygen exchange, resistive switching, $SrTiO_3$

Received: January 11, 2017
Revised: March 14, 2017
Published online: April 18, 2017

[1] ITRS, International Technology Roadmap for Semiconductors - 2013 Edition. **2013**.
[2] R. Waser, M. Aono, *Nat. Mater.* **2007**, *6*, 833.
[3] R. Waser, R. Dittmann, G. Staikov, K. Szot, *Adv. Mater.* **2009**, *21*, 2632.
[4] E. Linn, R. Rosezin, C. Kügeler, R. Waser, *Nat. Mater.* **2010**, *9*, 403.
[5] J. Borghetti, G. S. Snider, P. J. Kuekes, J. J. Yang, D. R. Stewart, R. S. Williams, *Nature* **2010**, *464*, 873.
[6] H.-S. P. Wong, H.-Y. Lee, S. Yu, Y.-S. Chen, Y. Wu, P.-S. Chen, B. Lee, F. T. Chen, M.-J. Tsai, *Proc. IEEE* **2012**, *100*, 1951.
[7] F. Miao, J. Joshua Yang, J. Borghetti, G. Medeiros-Ribeiro, R. Stanley Williams, *Nanotechnology* **2011**, *22*, 254007.
[8] D. S. Jeong, H. Schroeder, R. Waser, *Phys. Rev. B* **2009**, *79*, 195317/1.
[9] L. Goux, P. Czarnecki, Y. Y. Chen, L. Pantisano, X. P. Wang, R. Degraeve, B. Govoreanu, M. Jurczak, D. J. Wouters, L. Altimime, *Appl. Phys. Lett.* **2010**, *97*, 243509.
[10] H. Tian, H.-Y. Chen, G. Gao, S. Yu, J. Liang, Y. Yang, D. Xie, J. F. Kang, T.-L. Ren, Y. Zhang, H.-S. P. Wong, *Nano Lett.* **2013**, *13*, 651.
[11] M. Moors, K. K. Adepalli, Q. Lu, A. Wedig, C. Bäumer, K. Skaja, B. Arndt, H. L. Tuller, R. Dittmann, R. Waser, B. Yildiz, I. Valov, *ACS Nano* **2016**, *10*, 1481.
[12] R. Muenstermann, T. Menke, R. Dittmann, R. Waser, *Adv. Mater.* **2010**, *22*, 4819.
[13] Y. S. Kim, J. Kim, M. J. Yoon, C. H. Sohn, S. B. Lee, D. Lee, B. C. Jeon, H. K. Yoo, T. W. Noh, A. Bostwick, E. Rotenberg, J. Yu, S. D. Bu, B. S. Mun, *Appl. Phys. Lett.* **2014**, *104*, 13501/1.
[14] M. Kubicek, R. Schmitt, F. Messerschmitt, J. L. M. Rupp, *ACS Nano* **2015**, *9*, 10737.
[15] R. Dittmann, R. Muenstermann, I. Krug, D. Park, T. Menke, J. Mayer, A. Besmehn, F. Kronast, C. M. Schneider, R. Waser, *Proc. IEEE* **2012**, *100*, 1979.
[16] X. Sun, G. Li, L. Chen, Z. Shi, W. Zhang, *Nanoscale Res. Lett.* **2011**, *6*, 599/1.

[17] C. Baeumer, C. Schmitz, A. H. H. Ramadan, H. Du, K. Skaja, V. Feyer, P. Muller, B. Arndt, C. Jia, J. Mayer, R. A. De Souza, C. Michael Schneider, R. Waser, R. Dittmann, *Nat. Commun.* **2015**, *6*, 9610.
[18] S. Mildner, M. Beleggia, D. Mierwaldt, T. W. Hansen, J. B. Wagner, S. Yazdi, T. Kasama, J. Ciston, Y. Zhu, C. Jooss, *J. Phys. Chem. C* **2015**, *119*, 5301.
[19] D.-H. Kwon, K. M. Kim, J. H. Jang, J. M. Jeon, M. H. Lee, G. H. Kim, X.-S. Li, G.-S. Park, B. Lee, S. Han, M. Kim, C. S. Hwang, *Nat. Nanotechnol.* **2010**, *5*, 148.
[20] J. Kwon, A. A. Sharma, J. A. Bain, Y. N. Picard, M. Skowronski, *Adv. Funct. Mater.* **2015**, *25*, 2876.
[21] P. Gao, Z. Wang, W. Fu, Z. Liao, K. Liu, W. Wang, X. Bai, E. Wang, *Micron* **2010**, *41*, 301.
[22] G.-S. Park, Y.-B. Kim, S. Y. Park, X. S. Li, S. Heo, M. J. Lee, M. Chang, J. H. Kwon, M. Kim, U.-In Chung, R. Dittmann, R. Waser, K. Kim, *Nat. Commun.* **2013**, *4*, 2382.
[23] J. Norpoth, S. Mildner, M. Scherff, J. Hoffmann, C. Jooss, *Nanoscale* **2014**, *6*, 9852.
[24] Z. Liao, P. Gao, X. Bai, D. Chen, J. Zhang, *J. Appl. Phys.* **2012**, *111*, 114506.
[25] J. Chen, C. Huang, C. Chiu, Y. Huang, W. Wu, *Adv. Mater.* **2015**, *27*, 5028.
[26] R. J. Kamaladasa, A. A. Sharma, Y. Lai, W. Chen, P. A. Salvador, J. A. Bain, M. Skowronski, Y. N. Picard, *Microsc. Microanal.* **2015**, *21*, 140.
[27] D. H. Pearson, C. C. Ahn, B. Fultz, *Phys. Rev. B* **1993**, *47*, 8471.
[28] A. Ohtomo, D. A. Muller, J. L. Grazul, H. Y. Hwang, *Nature* **2002**, *419*, 378.
[29] C. Baeumer, C. Schmitz, A. Marchewka, D. N. Mueller, R. Valenta, J. Hackl, N. Raab, S. P. Rogers, M. I. Khan, S. Nemsak, M. Shim, S. Menzel, C. M. Schneider, R. Waser, R. Dittmann, *Nat. Commun.* **2016**, *7*, 12398.
[30] D. A. Muller, N. Nakagawa, A. Ohtomo, J. L. Grazul, H. Y. Hwang, *Nature* **2004**, *430*, 657.
[31] M. Abbate, F. M. F. de Groot, J. C. Fuggle, A. Fujimori, Y. Tokura, Y. Fujishima, O. Strebel, M. Domke, G. Kaindl, J. van Elp, B. T. Thole, G. A. Sawatzky, M. Sacchi, N. Tsuda, *Phys. Rev. B: Condens. Matter Mater. Phys.* **1991**, *44*, 5419.
[32] C. Lenser, M. Patt, S. Menzel, A. Köhl, C. Wiemann, C. M. Schneider, R. Waser, R. Dittmann, *Adv. Funct. Mater.* **2014**, *24*, 4466.
[33] K. Shibuya, R. Dittmann, S. Mi, R. Waser, *Adv. Mater.* **2010**, *22*, 411.
[34] E. Mikheev, J. Hwang, A. P. Kajdos, A. J. Hauser, S. Stemmer, *Sci. Rep.* **2015**, *5*, 11079.
[35] R. Schafranek, S. Payan, M. Maglione, A. Klein, *Phys. Rev. B* **2008**, *77*, 195310.
[36] S. H. Jeon, B. H. Park, J. Lee, B. Lee, S. Han, *Appl. Phys. Lett.* **2006**, *89*, 42904.
[37] A. Marchewka, D. Cooper, C. Lenser, S. Menzel, H. Du, R. Dittmann, R. E. Dunin-Borkowski, R. Waser, *Sci. Rep.* **2014**, *4*, 6975.
[38] F. A. Kroeger, *The Chemistry of Imperfect Crystals*, Wiley Interscience, New York, **1964**.
[39] R. Bruchhaus, C. R. Hermes, R. Waser, *MRS Online Proc. Libr.* **2011**, *1337*, 73.
[40] J. S. Lee, S. B. Lee, B. Kahng, T. W. Noh, *Appl. Phys. Lett.* **2013**, *102*, 253503/1.
[41] S. Lee, J. S. Lee, J.-B. Park, Y. K. Kyoung, M.-J. Lee, T. W. Noh, *APL Mater.* **2014**, *2*, 066103.
[42] A. Marchewka, R. Waser, S. Menzel, in *2015 Int. Conf. on Simulation of Semiconductor Processes and Devices (SISPAD)*, IEEE, Washington, DC, USA **2015**, *297*.
[43] W. C. Chueh, S. M. Haile, *Annu. Rev. Chem. Biomol. Eng.* **2012**, *3*, 313.
[44] R. Schmiedl, V. Demuth, P. Lahnor, H. Godehardt, Y. Bodschwinna, C. Harder, L. Hammer, H. P. Strunk, M. Schulz, K. Heinz, *Appl. Phys. A* **1996**, *62*, 223.
[45] A. Grill, W. Kane, J. Viggiano, M. Brady, R. Laibowitz, *J. Mater. Res.* **1992**, *7*, 3260.
[46] D. S. Jeong, H. Schroeder, U. Breuer, R. Waser, *J. Appl. Phys.* **2008**, *104*, 123716/1.
[47] R. Yang, K. Terabe, T. Tsuruoka, T. Hasegawa, M. Aono, *Appl. Phys. Lett.* **2012**, *100*, 231603/1.
[48] Y. Wang, X. Qian, K. Chen, Z. Fang, W. Li, J. Xu, *Appl. Phys. Lett.* **2013**, *102*, 042103.
[49] A. Mehonic, M. Buckwell, L. Montesi, M. S. Munde, D. Gao, S. Hudziak, R. J. Chater, S. Fearn, D. McPhail, M. Bosman, A. L. Shluger, A. J. Kenyon, *Adv. Mater.* **2016**, *28*, 7486.
[50] C. Baeumer, N. Raab, T. Menke, C. Schmitz, R. Rosezin, P. M. Müller, M. Andrä, V. Feyer, R. Bruchhaus, F. Gunkel, C. M. Schneider, R. Waser, R. Dittmann, *Nanoscale* **2016**, *8*, 13967.
[51] R. Ortega-Hernandez, M. Coll, J. Gonzalez-Rosillo, A. Palau, X. Obradors, E. Miranda, T. Puig, J. Sune, *Microelectron. Eng.* **2015**, *147*, 37.
[52] M. Scherff, B. Meyer, J. Hoffmann, C. Jooss, M. Feuchter, M. Kamlah, *New J. Phys.* **2015**, *17*, 033011.
[53] A. Wedig, M. Luebben, D.-Y. Cho, M. Moors, K. Skaja, V. Rana, T. Hasegawa, K. Adepalli, B. Yildiz, R. Waser, I. Valov, *Nat. Nanotechnol.* **2016**, *11*, 67.
[54] C. Y. Chen, L. Goux, A. Fantini, A. Redolfi, G. Groeseneken, M. Jurczak, in *2016 IEEE 8th International Memory Workshop (IMW)*, IEEE, Paris, France **2016**, 1.
[55] W. Kim, S. Menzel, D. J. Wouters, Y. Guo, J. Robertson, B. Rösgen, R. Waser, V. Rana, *Nanoscale* **2016**, *8*, 17774.

